Generation of a Retina Reporter hiPSC Line to Label Progenitor, Ganglion, and Photoreceptor Cell Types

Phuong T. Lam, Christian Gutierrez, Katia Del Rio-Tsonis and Michael L. Robinson*

Department of Biology and Center for Visual Sciences, Miami University, Oxford, OH 45056

*Corresponding author

Grant information:

This work was supported by grants from the Sigma Xi- Scientific Research Society (P.T.L. G201510151661206, G2017031589218117, G2018031589218117, Miami University Academic Challenge (P.T.L), Miami University College of Arts and Science (K.D.R.T. and M.L.R.), The James and Beth Lewis Endowed Professorship (M.L.R.), and National Eye Institute grant EY026816 (K.D.R.T). The FACS-Melody system was acquired with an NSF MRI grant 1726645 (M.L.R.).

Word count:

Title: 102 characters / 150 characters limit

Structure abstract: 247 words / 250 words limit

Text:

Introduction: 432 words

Method: 1,034 words

Results: 1,115 words

Discussion: 919 words

ABSTRACT

Purpose: Early in mammalian eye development, *VSX2, BRN3b*, and *RCVRN* expression marks neural retinal progenitors (NRPs), retinal ganglion cells (RGCs), and photoreceptors (PRs), respectively. The ability to create retinal organoids from human induced pluripotent stem cells (hiPSC) holds great potential for modeling both human retinal development and retinal disease. However, no methods allowing the simultaneous, real-time monitoring of multiple specific retinal cell types during development currently exist.

Method: CRISPR/Cas9-mediated homology directed repair (HDR) in hiPSCs facilitated the replacement of the *VSX2* (Progenitor), *BRN3b* (Ganglion), and *RCVRN* (Photoreceptor) stop codons with sequences encoding a viral P2A peptide fused to Cerulean, green fluorescent protein (GFP), and mCherry reporter genes, respectively, to generate a triple transgenic reporter hiPSC line called PGP1. This was accomplished by co-electroporating HDR templates and sgRNA/Cas9 vectors into hiPSCs followed by antibiotic selection. Functional validation of the PGP1 hiPSC line included the ability to generate retinal organoids, with all major retinal cell types, displaying the expression of the three fluorescent reporters consistent with the onset of target gene expression. Disaggregated organoids were also analyzed by FACS and fluorescent populations were tested for the expression of the targeted gene.

Results: Retinal organoids formed from the PGP1 line expressed appropriate fluorescent proteins consistent with the differentiation of NRPs, RGCs, and PRs. Organoids produced from the PGP1 line expressed transcripts consistent with the development of all major retinal cell types.

Conclusion and Translational Relevance: The PGP1 line offers a powerful new tool to study retinal development, retinal reprogramming, and therapeutic drug screening.

47

INTRODUCTION

Stem cells provide multiple avenues to address irreversible vision loss associated with retinal cell death caused by trauma or by disease. Common diseases including age-related macular degeneration (AMD) and glaucoma lead to irreversible blindness costing billions of dollars in social welfare and lost productivity[1,2]. Recent advancements in 3D-culture have led to the development of retinal organoids consisting of all major retinal cell types from human induced pluripotent stem cells (hiPSCs)[3]. These hiPSC-derived organoids can model normal neural retinal (NR) development and progression of retinal disease. Additionally, organoids provide a platform to screen drugs for the treatment of retinal degeneration[3,4]. Finally, hiPSCs can potentially make unlimited numbers of specific retinal neurons for transplantation therapies.

The rapidly expanding use of hiPSCs to model human retina justifies the need for tools to monitor the appearance of specific cell types without interrupting normal development. For this purpose, CRISPR/Cas9 gene editing facilitates the insertion of cell-type-specific reporters into hiPSCs. Although several hiPSCs with single reporter knock-ins exist[5–7], these lines only detect terminally differentiated retinal cell types, which limits the ability to study progression of retinal development in real-time. Having multiple cell type reporters inserted into the same genome will permit specific cell sorting and allow for the optimization of protocols that enrich for the development of particular retinal cell types. For example, one might need a large number of photoreceptors (PRs) or retinal ganglion cells (RGCs) to screen for drugs to treat AMD or glaucoma, respectively[8,9].

To address these limitations, we utilized CRISPR/Cas9 to insert reporter genes encoding fluorescent proteins into the *VSX2, BRN3b* and *RCVRN* loci in hiPSCs to make it possible to monitor the differentiation of NRPs, RGCs, and PR cells, respectively. *VSX2* encodes a

transcription factor that marks NRPs[10]. In the mature NR, only post-mitotic bipolar cells express *VSX2*[11-13]. RGCs represent the first mature NR cell type to develop and most RGCs express the BRN3b transcription factor[12]. PRs (rods and cones) express *RCVRN*, a protein important in the recovery phase of visual excitation[14]. The cell-type-specific expression pattern of these genes made them appropriate targets for fluorescent protein expression. Given their importance in retinal development and/or function, we sought to retain the function of both alleles of all three (*VSX2, BRN3b* and *RCVRN*) genes in engineered hiPSCs by utilizing viral P2A peptides to create fusion genes between the target and the fluorescent reporter that would self-cleave upon translation[15]. Therefore, we inserted a P2A:Cerulean reporter into the *VSX2* locus, a P2A:eGFP reporter into the *BRN3b* locus and a P2A:mCherry reporter into the *RCVRN* locus, by replacing the stop codon of the endogenous gene with the P2A:reporter.

METHODS

Specific Single Guide RNA Vector (sgRNA) Design: CRISPR specific guide RNAs (Table S1) were individually cloned into a PX458 vector that includes the *S. pyogenes* Cas9 (Addgene, #48138) as described[16]. To determine Cas9-sgRNA cutting efficiency, we transfected each vector into Human Embryonic Kidney (HEK293) cells. After 48 hours, HEK293 DNA was extracted and amplified by Q5 High-Fidelity PCR (NEB, M0494S) using primers encompassing the sgRNA recognition site. The PCR products were digested with T7 Endonuclease I (NEB, M0302S) as described[17]. Successful Cas9 cleavage by sgRNAs resulted in two distinct bands in the T7E1 assay.

Homology Directed Repair (HDR) Template Generation: To generate the HDR templates, the left and right HAs of each locus were amplified from the wild-type (WT) hiPSC

genomic DNA (see Table S2). The amplified HAs of *VSX2*, *BRN3b*, and *RCVRN* genes were inserted into the previously assembled vectors FRT.TK.Puro.FRT.pL451; LoxP.TK.Blast.LoxP.pL452, and FRT.TK.Neo.FRT.pL451 via Gibson Assembly (NEB, E2611L[18]), respectively (vector sequences available upon request). These insertions were confirmed by DNA sequencing. The Cerulean fluorescent reporter gene was derived from pCS-membrane-CeruleanFP, a gift from Sean Megason (Addgene plasmid # 53749)[19]. The GAP43-eGFP reporter gene was derived from pCAG-mGFP, a gift from Connie Cepko (Addgene plasmid #14757)[20]. The mCherry reporter gene was derived from pEF6V5:eGFP-CAAX-2A-mCherry, a gift from Steven Leach (Addgene plasmid 26901)[21].

Insertion of Fluorescent Reporter Genes into Selected Loci: To generate the RCVRN/mCherry hiPSCs, we transfected 2.5µg of the HDR template and 2.5µg of the sgRNA vector into WT hiPSCs (hiPSC6.2[22,23] from Life Technologies, A18945) using a 4D-Nucleofector-X-Unit and the P3-Primary-kit (Amaxa, V4XP-3012) based on manufacturer's protocol. After transfection, cells were cultured with Essential 8 media plus 10µM ROCK inhibitor (Sigma SCM075) overnight, with subsequent daily media changes without ROCK inhibitor. Antibiotic selection began after 48 hours with 100 µg/ml and slowly increased to 250 µg/ml of G418 (Corning, 30234CR) over the course of one week. DNA from resistant clones was extracted (Zymo Research, D3025), and screened for reporter integration by PCR and validated by DNA sequencing. A single RCVRN/mCherry hiPSC line was transfected with 1.25ug each of: the BRN3b:eGFP HDR template, the sgRNA vector to the *BRN3b* locus, the VSX2:Cerulean HDR template, and the sgRNA vector to the *VSX2* locus using nucleofection as described above. Double antibiotic selection was performed using 100 µg/ml each of blasticidin (InvivoGen, ant-bl-05) and puromycin (InvivoGen, ant-pr-1), and slowly increased up to 250

μg/ml of each antibiotic over the course of one week to select for blasticidin/puromycin resistant colonies. All resistant clones were screened for reporter integration by PCR (see Table S2) and validated by DNA sequencing.

Off-Target Screening: The PGP1 line was screened by selecting five high scoring off-target sites for each sgRNA provided by Benchling[24]. Each potential sgRNA off target site (Table S3) was screened by High-Fidelity PCR (Q5 NEB, M0491L) with primers listed in Table S4 and PCR products were sequenced by Eurofins Genomics. Each result was independently repeated five times.

3-D Retinal Organoid Generation from the PGP1 Triple Targeted Line: PGP1 retinal organoids were created using the Zhong et al., 2014 protocol with modification[25]. Briefly, hiPSCs were incubated in 0.5mM EDTA/DPBS (ThermoFisher, 15575020) for 5 minutes at 37^0 C, prior to dissociation and culturing in mTeSR1 (Stemcell, 85850) with 10 μM ROCK inhibitor (Sigma SCM075) to form aggregates. The aggregates were gradually transitioned into neural induction medium (NIM)[25] from D1-3 of differentiation, then cultured in NIM from D3 to D6. On D7, the aggregates were seeded on Matrigel (hESC-qualified, Corning 354277)-coated dishes in NIM at an approximate density of 20 aggregates per cm^2 and switched to DMEM/F12 (ThermoFisher, 11320082) (3:1) supplemented with 2% Gem21 NeuroPlex (without vitamin A, Gemini, 400-161), 1X NEAA, and 1% antibiotic-antimycotic (Thermo,15240062) on D16, with medium changes every third day. On D28 of differentiation, cells were detached, transferred to Petri dishes, and cultured in suspension in DMEM/F12 (3:1) supplemented with 2% Gem21 NeuroPlex, 1X NEAA (ThermoFisher, 11140050), and 1% antibiotic-antimycotic (ThermoFisher, 15240096). Within 3-5 days, cells began forming 3-D retinal organoids. The organoids were then mechanically separated from the rest of the cells using sharpened tungsten

needles under a dissecting microscope. From that point on, the medium was changed twice a week. To culture the retinal organoids long-term, the medium was supplemented with 10% fetal bovine serum (FBS) (Gibco, 26140079), and 2 mM GlutaMax (Invitrogen, 35050061) beginning on D42.

Reverse Transcription-PCR (RT-qPCR) Analysis of Retinal Organoids: RNA isolation of retinal organoids was done using Quick RNA miniprep (Zymo Research, R1057). Reverse transcription was performed using the ImProm-II Reverse Transcription System (Promega, A3800). RT-qPCR was performed with GoTaq® qPCR Master Mix (Promega, A6001) using a CFX Connect Bio-Rad qPCR System. Forty cycles were run at 95 °C denaturation for 40 s, 60 °C annealing for 40 s and 72 °C extension for 60 s, using primers listed in Table S5. The expression levels of genes were normalized to GAPDH mRNA levels and analyzed using the delta-delta Ct method with significant differences revealed by a two tailed Student's t-test. Error bars in each figure represents the standard error of the mean (SE) of three individual experiments.

Immunofluorescence of the Retinal Organoids: Organoids were fixed with 4% paraformaldehyde (FisherSci, 15710) for 20 minutes at room temperature, incubated in 30% sucrose overnight at 4ºC and embedded in OCT (VWR, 95057-838). Organoids were cryosectioned at 15 μm and immunofluorescence was performed using antibodies listed in Table S6 with images acquired using a Nikon Eclipse 80i microscope or Zeiss LSM 710 Laser Scanning Confocal System. Residual fluorescence from the fluorescent proteins failed to survive our fixation and embedding protocol and therefore did not interfere with immunofluorescence studies (Fig. S1, S2).

Fluorescence-Activated Cell Sorting (FACS) Analysis of the Retinal Organoids: Thirty organoids each from D55 and D135 were enzymatically dissociated in Accutase (Innovative Cell Technologies, AT104), and filtered through a 40 µm strainer (Fishersci, 22-363-547) to get single cells, and resuspended in ice cold 5%FBS/1xHBSS (Fishersci, 14-025-092) at a concentration of 10 million cells/ml. These cells were filtered again through a second strainer (Fisher, 08-771-23) prior to sorting. At D55, single cells were sorted for Cerulean positive (Cerulean^{+}) and negative (Cerulean^{-}) populations, as well as the eGFP positive (eGFP^{+}) and negative (eGFP^{-}) populations using a FACSMelody Cell Sorter (BD Biosciences). For the D135, single cells were sorted for mCherry positive (mCherry^{+}) and negative (mCherry^{-}) populations. The sorted populations were used to measure mRNA transcripts for Cerulean*, VSX2,* eGFP*, BRN3b,* mCherry*, RCVRN,* and *GAPDH* via RT-qPCR (Table S7). Gates for sorting disaggregated retinal organoids were established in a previous experiment using HEK293 cells transiently transfected with an expression plasmid for Cerulean, eGFP, or mCherry. FACS was conducted 48 hours after transfection to determine the appropriate gates for each fluorescent protein (Fig. S3). In addition, organoids produced from WT hiPSCs were used to established negative gates.

RESULTS

Creation of the Neural Retinal Progenitor/ Retinal Ganglion/ Photoreceptor (PGP1) Reporter: CRISPR/Cas9 mediated homology directed repair (HDR, Fig. 1 A) facilitated the replacement of the endogenous stop codons of the *VSX2*, *BRN3b* and *RCVRN* genes with a P2A peptide fused to a fluorescent reporter gene. Briefly, hiPSCs were nucleofected with a *S. pyogenes* Cas9 expression vector (containing appropriate sgRNAs) and HDR templates targeting

each locus. Antibiotic resistant clones were tested by DNA sequence analysis of two PCR amplicons (Table S8) encompassing the 5' and 3' ends of the targeted modification with at least one PCR primer outside of the homology arm (HA) (Fig. 1 B-D). The *RCVRN* locus was first targeted independently, resulting in 48 G418 resistant hiPSC clones, with three (6.25%) clones verified as correctly targeted by DNA sequencing of PCR amplicons (Fig. 1 D). Simultaneous targeting of the *VSX2* and *BRN3b* loci from one of these clones yielded 144 clones resistant for both puromycin and blasticidin. PCR genotyping followed by DNA sequencing identified four (2.8%) of these triple antibiotic resistant clones (56, 101, 108 and 122) as correctly targeted at all three targeted loci. We randomly designated one (122) of these triple targeted hiPSC clones (PGP1) for further molecular and functional analyses.

A three-primer PCR strategy, utilizing the forward primer outside 5'HA, with two different reverse primers made it possible to determine if the PGP1 line was heterozygous or homozygous at each locus. All three loci yielded PCR amplicons with expected band sizes for wild-type (WT) and targeted alleles (Fig. 2). Sequence analysis from the WT PGP1 alleles failed to reveal indel mutations at the sgRNA cut sites (Fig. S4). Additionally, DNA sequencing of PCR fragments, amplified by primers surrounding predicted high-scoring off-target sites for each sgRNA, revealed no off-target mutations in PGP1 (Table S3).

Functional Analysis of the Fluorescent Reporters in the PGP1: To test the function of PGP1 retinal reporter genes, we created retinal organoids from PGP1.hiPSCs, using a previously described protocol[16]. Only the VSX2:Cerulean reporter expressed at day 20 (D20) of differentiation with fluorescence restricted to developing eye field domains (Fig. S5). Manually isolated eye field domains (isolated between D20 and D24), formed spherical cups (Fig. S6) with both Cerulean and eGFP expression by D55 (Fig. 3 A, B). In the BRN3b reporter, the eGFP

contained a GAP43 palmitoylation tag derived from the plasmid pCAG-mGFP to drive eGFP to the cell membrane[26], which highlighted RGC axon bundles (Fig. 3 B, D). At D55, sparse mCherry fluorescence, driven by *RCVRN* promoter, appeared sporadically throughout the organoids (Fig. 3 C, D). A merged image of all three signals shows the restriction of fluorescent expression to distinct cells with little evidence of overlapping reporter expression (Fig. 3 D, Supplemental Movie). Scanning parameters for Fig. 3 and the Supplemental Movie are supplied in Table S9.

As the organoids matured, the ratio of cells expressing different fluorescent proteins changed. At D55, the majority of cells in the organoid express Cerulean, but as the organoids mature, the proportion of Cerulean expressing cells decreases (Fig. 3 A, E, I). By D95, the eGFP-expressing axon bundles had disappeared, but punctate eGFP staining remained within the organoid and overall eGFP expression declined by D135 (Fig. 3 F, J). This real-time decline in eGFP expression at later stages of organoid development correlates with the decline in the BRN3b mRNA levels (Fig. 5E). Other laboratories have noted the challenge of long-term survival of retinal ganglion cells in 3-D retinal organoid culture[27,28]. The loss of eGFP-expressing retinal ganglion cell axon bundles in organoid culture may relate to a lack of synaptic contact to target brain regions[29,30]. Although only weak mCherry fluorescence appeared at D55, mCherry expression increased such that by D135 large areas of the organoid displayed mCherry fluorescence (Fig. 3 C, G, K). Cerulean, eGFP and mCherry signals did not appear to overlap, either in the whole mounts, nor in the optical section Z-stack (supplemental movie).

To confirm that the observed fluorescent proteins identified the targeted cell types, we sorted organoid cells based on fluorescent protein expression. At D55, the organoids contained large numbers of Cerulean and $eGFP^+$ cells, but relatively fewer $mCherry^+$ cells. By D135, the

organoids contained abundant mCherry^{+} cells. Considering this, we performed FACS on single cell suspensions to collect Cerulean^{+} and eGFP^{+} (Fig. 4 A, D) cells from D55 and mCherry^{+} (Fig. 4 G) cells from D135 organoids. At D55, Cerulean^{+} and eGFP^{+} cells comprised approximately 11.3% and 4.9% of the single cells from disaggregated organoids. At D135, approximately 53% of organoid cells were mCherry^{+}. We also sorted organoids from WT hiPSCs using the same gates used for the PGP1-derived organoids and found no cells within the Cerulean (Fig. 4 J), eGFP (Fig. 4 K) or mCherry (Fig. 4 L) gates. Since FACS can only analyze single cells, it remains possible that certain organoid cell types exhibit increased resistance to single cell dissociation that could bias our quantitative analysis. However, this bias should not influence comparative analysis between expressing and non-expressing cells for any single fluorescent protein.

We performed RT-qPCR and immunofluorecence to determine if fluorescent reporter expression correlated with the expression of the targeted gene in sorted samples. The transcript analysis revealed that the sorted Cerulean^{+} population (Fig. 4 A) expressed significantly more Cerulean mRNA than the Cerulean^{-} population (Fig. 4 B). Likewise, the Cerulean^{+} population expressed approximately 3 times more *VSX2* mRNA than the Cerulean^{-} population (Fig. 4 C). The eGFP^{+} sorted population (Fig. 4 D) expressed 22-fold more eGFP mRNA and 9.1-fold more *BRN3b* mRNA than the eGFP^{-} population (Fig. 4 E, F). On D135, the mCherry^{+} (Fig. 4 G) population expressed approximately 4.9 times more mCherry mRNA and 1.9 times more *RCVRN* mRNA than the mCherry^{-} population (Fig. 4 H, I). For *VSX2* and *BRN3b*, the majority of expressing cells appeared in the Cerulean^{+} and eGFP^{+} populations, respectively. The appearance of relatively more *RCVRN* transcripts in the mCherry^{-} population than *BRN3b* transcripts in the eGFP^{-} or *VSX2* transcripts in the Cerulean^{-} populations, suggests that not all RCVRN-expressing

cells express mCherry. Double immunohistochemical analysis of D55 organoids revealed co-labeling of BRN3 and GFP (Fig. S7 A-C), while D163 organoids showed co-labeling of VSX2 and GFP (Fig. S7 D-F). Note that in both of the above cases our antibody cannot distinguish GFP from Cerulean. Although antibodies for RCVRN co-label cells that express mCherry in D163 organoids (Fig. S7 G-I), the organoids exhibited some RCVRN-expressing cells that failed to express mCherry. However, this same analysis showed that all $mCherry^{+}$ cells co-express RCVRN. The $RCVRN^{+}/mCherry^{-}$ proportion of cells exhibited organoid to organoid variability (Fig. S8). All of the positive and negative sorted populations for each fluorescent protein were tested by RT-qPCR in triplicate (Fig 4 B, C, E, F, H, I). These data demonstrate that the reporters faithfully reveal the target gene-expressing cells. Although we did not conduct FACS analyses on organoids formed by any of the other triple targeted hiPSC lines, we did confirm that clones 56 and 101, in addition to PGP1 (122) formed organoids expressing all three fluorescent proteins.

PGP1-Derived Retinal Organoids Contain All Major Retinal Cell Types: a comparison of transcripts expressed by PGP1 hiPSCs at D0 of differentiation with those expressed by PGP1-derived retinal organoids at D55 revealed a decrease in pluripotency-related genes and an increase in retinal differentiation-related genes. Pluripotency transcripts for *OCT4* (*POU5F1*) and *NANOG* expressed abundantly at D0 (Fig. 5 A). In contrast, the NRP transcripts (*PAX6*, *SIX3*, and *LHX2*) (Fig. 5 B) and retinal pigment epithelium (RPE) (*MITF* and *BEST1*) (Fig. 5 C) increased significantly during early retinal organoid differentiation at D55. In addition, a sequential expression of NRPs (*VSX2*) and RGCs (*BRN3b*) revealed a decline, while the level of PRs transcript (*RCVRN*) increased significantly from D55 to D166 of differentiation (Fig. 5 D, E, F).

PGP1-derived organoids contained cells of all major retinal cell types. At D55, organoids expressed the eye field precursor protein RX (Fig. 6 A), NRP markers: PAX6, SIX3, VSX2 (Fig. 6 B, C, D), and the proliferation marker MCM2 (Fig. 6 E) throughout the D55 organoid tissue. In contrast, the expression of BRN3b (marking RGCs), localized interiorly (outlined in Fig. 6 F), as did AP2-α (amacrine cell marker) by D70 (outlined Fig. 6 G). Although RCVRN (PR marker), initially appeared throughout the organoid, by D70 RCVRN appeared near the organoid periphery (Fig. 6 H). At D95, PROX1 (horizontal cell marker), was located below the putative outer nuclear layer (Fig. 6 I). CRALBP, a marker of the late-differentiating Müller glia cells, appeared through the full thickness of the retinal organoids at D163 (Fig. 6 J). Although VSX2 expression initially characterizes proliferating (MCM2 positive) NRP cells, VSX2 appears later in non-proliferating (MCM2 negative) bipolar cells. These VSX2 positive/MCM2 negative bipolar cells increase in abundance by D163 (Fig. 6 K, L).

DISCUSSION

We created an hiPSC line (PGP1) for real-time analysis of NR differentiation with multiple retinal cell-type-specific reporters via CRISPR/Cas9 genome editing. Furthermore, we functionally characterized PGP1 both by fluorescent protein expression and by differentiation into all major retinal cell types during retinal organoid formation. Although previous reports described single retinal cell-type-specific reporters, to our knowledge, PGP1 represents the first triple targeted retinal reporter hiPSC line[5–7]. The ability of the PGP1 to facilitate visual observation of retinal differentiation, without compromising retinal organoid formation typical of WT hiPSCs[25], makes this clone particularly useful for several applications.

PGP1 provides a powerful tool for real-time retinal disease modeling. For example, hiPSC-derived organoids from patients with mutations leading to retinitis pigmentosa and Leber

congenital amaurosis have provided important insights about the pathobiology of these diseases[31-34]. Likewise, RGCs with specific mutations, differentiated from patient-derived hiPSCs, have provided models for optic atrophy and glaucoma[35,36]. The relative ease of creating specific mutations with CRISPR/Cas9 genome editing should make it possible to take advantage of the cell-type-specific reporters in PGP1 when modeling genetic retinal diseases[32].

PGP1-derived retinal organoids will provide a platform to screen drugs to treat retinal damage. A number of different physical or chemical insults can result in PR injury, making the search for compounds that can prevent or minimize such damage very important. Retinal organoids made from mouse iPSCs, with a Nrl-eGFP reporter to label rod PRs, facilitated the testing of compounds to protect PRs from 4-hydroxytamoxifen-induced degeneration[37]. Additionally, the recently reported three-dimensional automated reporter quantification (3D-ARQ) technology[38] would make screening drugs that affect retinal development and/or survival straightforward in PGP1-derived organoids. Therefore, the use of PGP1 hiPSCs for such a purpose would have the added advantage of simultaneous real-time monitoring of NRPs and PRs without having to fix the organoid and terminate the experiment. In fact, the loss of fluorescence in the PGP1-derived organoids post-fixation (Fig. S1) presents a small limitation of using this line for terminal analysis. However, immunohistochemistry can reveal mCherry and GFP/Cerulean expression in fixed organoid tissue (Fig. S7). In fact, we consider the loss of reporter protein fluorescence post-fixation as an advantage since it removes a potentially interfering signal from subsequent immunohistochemical analysis with fluorescent secondary antibodies.

PGP1 hiPSCs will facilitate protocol optimization to achieve the differentiation and/or survival of specific retinal cell types. For example, improved mature PR yields and laminar

stratification resulted from the use of stirred-tank bioreactors, due to increased cell proliferation and decreased apoptosis[38]. This study used immunohistochemical and FACS-mediated immuno purification of organoid-derived cell types. PGP1-derived organoids would permit similar protocol optimization for multiple cell types in real-time without relying on antibody labels. Additionally, the decline of ganglion axon bundles in late-stage organoids observed in our line and other published observations [28-30] presents a challenge for culturing RGCs with our current organoid protocol. The PGP1-dervied organoids would permit protocol optimization for long-term survival of RGCs and axon bundles in late-stage organoids. Therefore, the ability to continuously monitor RGCs and PRs should improve optimization for long-term survival of these cell types.

PGP1 hiPSCs could provide an effective strategy for improved purification of specific cell types. In direct differentiation protocols to achieve particular retinal cell types from hiPSCs, purifying fully differentiated, mature cell types remain an issue[39]. The purification of specific retinal neurons can often facilitate downstream analysis, or for transplantation studies. Recombinant AAV viruses containing a GFP reporter driven by an L/M cone-specific promoter led to the successful FACS isolation of cone PRs from both human fetal retina and from hiPSC-derived retinal organoids[40]. A similar strategy used recombinant lentivirus to achieve GFP expression from the PR-specific (IRBP) promoter to achieve FACS purification of hiPSC-derived PR cells prior to transplantation into immunocompromised mice[41]. Although both of these reports relied on virus-mediated reporter gene expression, others have adopted the use of endogenous reporters. For example, hiPSCs engineered with a P2A peptide-mCherry reporter into the *BRN3b* locus facilitated the purification of viable RGCs from retinal organoids by FACS[5]. These examples all attest to the potential of the PGP1 line for purification of specific

retinal cell types. However, the unique feature of the PGP1 line lies in its potential for simultaneously purifying NRPs, RGCs, PRs and bipolar cells.

hiPSC lines with multiple cell-type-specific reporters could serve as a powerful tool for proof-of-concept studies and for tracking retinal specific cell fates post-transplantation in animal models. For example, transplanting human NRPs into a mouse glaucoma model increased host RGC survival[42]. In the future, PGP1-derived cells will make it possible to evaluate the fate of transplanted cells in animal models *in vivo*. In these transplants, PGP1-derived NRPs, and later bipolar cells, would exhibit blue fluorescence, while RGCs or PRs derived from the transplant would exhibit green or red fluorescence, respectively. In another study, transplantation of GFP-labeled human PRs into a rat model of retinitis pigmentosa demonstrated restoration of the host rod function[43]. Although these authors reported integration of GFP positive PRs into the outer nuclear layer, the recent realization of cytoplasmic transfer from donor to host cells in PR transplantation[44,45] necessitates further confirmation of donor cell integration. Transplantation of PGP1-derived NRPs into an animal model of retinal degeneration would only result in GFP+ ganglion cells or mCherry^{+} PRs if these NRPs differentiated into these cell types in situ. These experiments could provide more definitive proof of donor cell integration and could also serve as an indicator of both cell survival and cell fate of the transplanted NRPs.

In summary, we demonstrate a CRISPR/Cas9 strategy to target the expression of multiple fluorescent reporter genes into endogenous loci in hiPSCs. In doing so, we created a triple transgenic hiPSC line (PGP1) and tested the function of this line by directed differentiation into 3-D retinal organoids. Organoids produced from the PGP1 line expressed Cerulean in NRPs and bipolar cells, membrane-targeted eGFP in RGCs and mCherry in PRs. In addition, PGP1-derived retinal organoids contained all major retinal cell types. The usefulness of this strategy extends to

369 virtually any cell-type-specific gene, limited only by the number of different fluorescent
370 reporters available for simultaneous analysis. The PGP1 line, and subsequent hiPSC lines
371 developed using this approach, hold great promise for studying retinal development, disease
372 modeling, drug screening, and pre-clinical transplantation studies.
373

REFERENCES

1. Sowden, J. C. ESC-Derived Retinal Pigmented Epithelial Cell Transplants in Patients: So Far, So Good. *Cell Stem Cell* **15**, 537–538 (2014).
2. Veleri, S. *et al.* Biology and therapy of inherited retinal degenerative disease: insights from mouse models. *Dis. Model. Mech.* **8**, 109–129 (2015).
3. Llonch, S., Carido, M. & Ader, M. Organoid technology for retinal repair. *Dev. Biol.* **433**, 132–143 (2018).
4. DiStefano, T. *et al.* Accelerated and Improved Differentiation of Retinal Organoids from Pluripotent Stem Cells in Rotating-Wall Vessel Bioreactors. *Stem Cell Reports* **10**, 300–313 (2018).
5. Sluch, V. M. *et al.* Differentiation of human ESCs to retinal ganglion cells using a CRISPR engineered reporter cell line. *Sci. Rep.* **5**, 16595 (2015).
6. Sluch, V. M. *et al.* Enhanced Stem Cell Differentiation and Immunopurification of Genome Engineered Human Retinal Ganglion Cells. *Stem Cells Transl. Med.* **6**, 1972–1986 (2017).
7. Phillips, M. J. *et al.* Generation of a rod-specific NRL reporter line in human pluripotent stem cells. *Sci. Rep.* **8**, (2018).
8. Shirai, H. *et al.* Transplantation of human embryonic stem cell-derived retinal tissue in two primate models of retinal degeneration. *Proc. Natl. Acad. Sci. U. S. A.* **113**, E81–90 (2016).
9. Jin, Z.-B. *et al.* Modeling retinal degeneration using patient-specific induced pluripotent stem cells. *PLoS One* **6**, e17084 (2011).
10. Zou, C. & Levine, E. M. Vsx2 controls eye organogenesis and retinal progenitor identity via homeodomain and non-homeodomain residues required for high affinity DNA binding. *PLoS Genet.* **8**, e1002924 (2012).

11. Phillips, M. J. *et al.* Modeling human retinal development with patient-specific induced pluripotent stem cells reveals multiple roles for visual system homeobox 2. *Stem Cells* **32**, 1480–1492 (2014).
12. Badea, T. C., Cahill, H., Ecker, J., Hattar, S. & Nathans, J. Distinct roles of transcription factors brn3a and brn3b in controlling the development, morphology, and function of retinal ganglion cells. *Neuron* **61**, 852–864 (2009).
13. Polans, A. S. *et al.* Recoverin, a photoreceptor-specific calcium-binding protein, is expressed by the tumor of a patient with cancer-associated retinopathy. *Proc. Natl. Acad. Sci. U. S. A.* **92**, 9176–9180 (1995).
14. Cao, D. & Barrionuevo, P. A. Estimating photoreceptor excitations from spectral outputs of a personal light exposure measurement device. *Chronobiol. Int.* **32**, 270–280 (2015).
15. Wang, Y., Wang, F., Wang, R., Zhao, P. & Xia, Q. 2A self-cleaving peptide-based multi-gene expression system in the silkworm Bombyx mori. *Sci. Rep.* **5**, 16273 (2015).
16. Ran, F. A. *et al.* Genome engineering using the CRISPR-Cas9 system. *Nat. Protoc.* **8**, 2281–2308 (2013).
17. Vouillot, L., Thélie, A. & Pollet, N. Comparison of T7E1 and Surveyor Mismatch Cleavage Assays to Detect Mutations Triggered by Engineered Nucleases. *G3: Genes|Genomes|Genetics* **5**, 407–415 (2015).
18. Liu, P., Jenkins, N. A. & Copeland, N. G. A highly efficient recombineering-based method for generating conditional knockout mutations. *Genome Res.* **13**, 476–484 (2003).
19. Megason, S. G. In toto imaging of embryogenesis with confocal time-lapse microscopy. *Methods Mol. Biol.* **546**, 317–332 (2009).
20. Matsuda, T. & Cepko, C. L. Controlled expression of transgenes introduced by in vivo

electroporation. Proc. *Natl. Acad. Sci. U. S. A.* **104**, 1027–1032 (2007).

21. Provost, E., Rhee, J. & Leach, S. D. Viral 2A peptides allow expression of multiple proteins from a single ORF in transgenic zebrafish embryos. *Genesis* **45**, 625–629 (2007).

22. Burridge, P. W. *et al.* A universal system for highly efficient cardiac differentiation of human induced pluripotent stem cells that eliminates interline variability. *PLoS One* **6**, e18293 (2011).

23. Chen, G. *et al.* Chemically defined conditions for human iPSC derivation and culture. *Nat. Methods* **8**, 424–429 (2011).

24. Benchling · Better tools, faster research. Available at: https://benchling.com/crispr. (Accessed: 8th February 2018).

25. Zhong, X. *et al.* Generation of three-dimensional retinal tissue with functional photoreceptors from human iPSCs. *Nat. Commun.* **5**, 4047 (2014).

26. Gauthier-Kemper, A. *et al.* Interplay between phosphorylation and palmitoylation mediates plasma membrane targeting and sorting of GAP43. *Mol. Biol. Cell* **25**, 3284–3299 (2014).

27. DiStefano, T. et al. Accelerated and Improved Differentiation of Retinal Organoids from Pluripotent Stem Cells in Rotating-Wall Vessel Bioreactors. *Stem Cell Reports* **10**, 300–313 (2018)

28. Tanaka, T. et al. Generation of retinal ganglion cells with functional axons from human induced pluripotent stem cells. *Sci. Rep.* **5**, 8344 (2015)

29. Isenmann, S., Kretz, A. & Cellerino, A. Molecular determinants of retinal ganglion cell development, survival, and regeneration. *Prog. Retin. Eye Res.* **22**, 483–543 (2003).

30. Lom, B. & Cohen-Cory, S. Brain-derived neurotrophic factor differentially regulates retinal ganglion cell dendritic and axonal arborization in vivo. *J. Neurosci.* **19**, 9928–9938 (1999).

31. Parfitt, D. A. *et al.* Identification and Correction of Mechanisms Underlying Inherited Blindness in Human iPSC-Derived Optic Cups. *Cell Stem Cell* **18**, 769–781 (2016).
32. Schwarz, N. *et al.* Arl3 and RP2 regulate the trafficking of ciliary tip kinesins. *Hum. Mol. Genet.* **26**, 2480–2492 (2017).
33. Tucker, B. A. *et al.* Patient-specific iPSC-derived photoreceptor precursor cells as a means to investigate retinitis pigmentosa. *Elife* **2**, e00824 (2013).
34. Megaw, R. *et al.* Gelsolin dysfunction causes photoreceptor loss in induced pluripotent cell and animal retinitis pigmentosa models. *Nat. Commun.* **8**, 271 (2017).
35. Chen, J., Riazifar, H., Guan, M.-X. & Huang, T. Modeling autosomal dominant optic atrophy using induced pluripotent stem cells and identifying potential therapeutic targets. *Stem Cell Res. Ther.* **7**, 2 (2016).
36. Teotia, P. *et al.* Modeling Glaucoma: Retinal Ganglion Cells Generated from Induced Pluripotent Stem Cells of Patients with SIX6 Risk Allele Show Developmental Abnormalities. *Stem Cells* **35**, 2239–2252 (2017).
37. Ito, S.-I., Onishi, A. & Takahashi, M. Chemically-induced photoreceptor degeneration and protection in mouse iPSC-derived three-dimensional retinal organoids. *Stem Cell Res.* **24**, 94–101 (2017).
38. Ovando-Roche, P. *et al.* Use of bioreactors for culturing human retinal organoids improves photoreceptor yields. *Stem Cell Res. Ther.* **9**, 156 (2018).
39. Tano, K. *et al.* A novel in vitro method for detecting undifferentiated human pluripotent stem cells as impurities in cell therapy products using a highly efficient culture system. *PLoS One* **9**, e110496 (2014).
40. Welby, E. *et al.* Isolation and Comparative Transcriptome Analysis of Human Fetal and

iPSC-Derived Cone Photoreceptor Cells. *Stem Cell Reports* **9**, 1898–1915 (2017).

41. Lamba, D. A. *et al.* Generation, purification and transplantation of photoreceptors derived from human induced pluripotent stem cells. *PLoS One* **5**, e8763 (2010).

42. Ma, J. *et al.* Transplantation of Human Neural Progenitor Cells Expressing IGF-1 Enhances Retinal Ganglion Cell Survival. *PLoS One* **10**, e0125695 (2015).

43. Jayaram, H. *et al.* Transplantation of photoreceptors derived from human Muller glia restore rod function in the P23H rat. *Stem Cells Transl. Med.* **3**, 323–333 (2014).

44. Nickerson, P. E. B., Ortin-Martinez, A. & Wallace, V. A. Material Exchange in Photoreceptor Transplantation: Updating Our Understanding of Donor/Host Communication and the Future of Cell Engraftment Science. *Front. Neural Circuits* **12**, 17 (2018).

45. Ortin-Martinez, A. *et al.* A Reinterpretation of Cell Transplantation: GFP Transfer From Donor to Host Photoreceptors. *Stem Cells* **35**, 932–939 (2017).

AUTHOR CONTRIBUTION

P.T.L. designed and conducted all CRISPR/Cas9 targeting and screening of hiPSC lines, performed all immunohistochemistry and confocal microscopy, designed and conducted all RT-qPCR analysis and FACS sorting. C.G. conducted all retinal organoid cultures and assisted with immunohistochemistry. K.D.R.T. participated in experimental design and reviewed all of the data for the manuscript. M.L.R. supervised all experiments, participated in all aspects of experimental design, and reviewed all the data. P.T.L. and M.L.R. wrote the manuscript. All authors reviewed and edited the manuscript.

ACKNOWLEDGMENTS

We would like to acknowledge Brad D. Wagner and Dr. Paul James for technical assistance, and Dr. Timothy Wilson for assistance with FACS analysis. The authors acknowledge the assistance of both the Center for Bioinformatics and Functional Genomics and the Center for Advanced Microscopy and Imaging at Miami University. We would like to thank Stephanie Padula, Dr. Anthony Sallese, Nathan Burns and Adam LeFever for editing the manuscript prior to submission.

ADDITIONAL INFORMATION

Competing interest statement: A provisional United States patent application (62/660,590) for the PGP1 line was filed April 20, 2018. The terms of this arrangement are managed by Miami University in accordance with its Conflict of Interest policies. This does not alter authors' adherence to journal policies on sharing data and materials. Requests for PGP1 lines should be addressed to M.L.R (robinsm5@miamioh.edu). The authors declare no other competing and/or financial interests.

DATA AVAILABILITY STATEMENT

The authors will make all relevant data not included with the manuscript and supplemental materials freely available upon request.

FIGURE LEGENDS

Figure 1. Creation of the Neural Retinal Progenitor/ Retinal Ganglion Cell/ Photoreceptor (PGP1) Reporter hiPSC Line by CRISPR/Cas9 Genome Editing. (A) Schematic illustration of the generalized CRISPR/Cas9-mediated insertion strategy. CRISPR/Cas9-mediated the replacement of the endogenous STOP codon of *VSX2* (B), *BRN3b* (C), and *RCVRN* (D) loci with P2A:Cerulean, P2A:eGFP, and P2A:mCherry by homologous recombination in WT hiPSCs. Following nucleofection and triple antibiotic selection for Puromycin (PURO), Blasticidin (BLAST), and G418 (NEO) the resistant clones were screened by PCR with primer sets. (B) FW1/RV1 (forward primer (FW) located outside *VSX2* 5'HA and reverse primer (RV) located inside Cerulean) with the expected band size of 2.1kb, and FW2/RV2 (inside PURO to outside *VSX2* 3'HA) with the expected band size of 1.9kb. (C) FW3/RV3 (outside *BRN3b* 5'HA to inside membrane tagged eGFP) with the expected band size of 1.7kb; and FW4/RV4 (inside BLAST to outside *BRN3b* 3'HA) with the expected band size of 1.5kb. (D) FW5/RV5 (outside *RCVRN* 5'HA to inside mCherry) with the expected band size of 1.2kb; and FW6/RV6 (inside NEO to outside *RCVRN* 3'HA) with the expected band size of 1.5kb. The WT hiPSC was used as control where no bands were seen. All the positive PCR bands were verified by sequencing. The original gels that were cropped for clarity in this figure (with white spaces between non-adjacent lanes) can be seen in their entirety in Fig. S9. Primer information listed in Table S8.

Figure 2. Determining the Zygosity of the PGP1 Line. In each case, a three-primer PCR strategy determined whether the PGP1 line was homozygous or heterozygous at the targeted loci. For the *VSX2* locus, primer FW1 is located outside the *VSX2* 5'HA, RV1 is located inside Cerulean, and RV2 is located outside the *VSX2* 3'HA. (A) The un-edited *VSX2* allele (FW1/RV2) should generate a 2.6kb band, (A') while the edited *VSX2* allele (FW1/RV1) should generate a 2.1kb band. (A'') A gel image showed bands of 2.6kb and 2.1kb for the PGP1 line while the WT hiPSC showed a 2.6kb band indicating that PGP1 is heterozygous at the *VSX2* locus. For the *BRN3b* locus, FW3 is located outside the *BRN3b* 5'HA, RV3 is located inside the eGFP, and RV4 is located outside the *BRN3b* 3'HA. (B) The un-edited *BRN3b* allele (FW3/RV4) should generate a 2.4kb band, (B') while the edited *BRN3b* allele (FW3/RV3) should generate a band of 1.7kb. (B") A gel image showed bands of 2.4kb and a 1.7kb for the PGP1 line while the WT hiPSC showed only a 2.4kb band, showing that PGP1 is heterozygous at the *BRN3b* locus. For the *RCVRN* locus, FW5 is located outside the *RCVRN* 5'HA, RV5 is located inside mCherry, and RV6 is located outside the *RCVRN* 3'HA. (C) The un-edited *RCVRN* allele (FW5/RV6) should generate a 2.2kb band, (C') while the edited *RCVRN* allele (FW5/RV5) should generate a 1.2kb band. (C") A gel image showed bands of 2.2kb and a 1.2kb for the PGP1 line while the WT hiPSC showed only a 2.2kb band, indicating that PGP1 is heterozygous at the *RCVRN* locus. The original gels that were cropped for clarity in this figure (with white spaces between non-adjacent lanes) can be seen in their entirety in Fig. S10. Primer information listed in Table S8.

Figure 3. Functional Analysis of the Fluorescent Reporters in the PGP1 Line via Retinal Organoid Formation. Single three-dimensional retinal organoids derived from the PGP1 hiPSC line were visualized by fluorescent microscopy at D55 (A, B, C, D), D95 (E, F, G, H) and D135 (I, J, K, L) of differentiation. Organoids were visualized with a 458 nm laser to excite Cerulean,

driven by the *VSX2* promoter (A, E, I), a 488 nm laser to excite eGFP driven by the *BRN3b* promoter (B, F, J) and both 543 nm and 633 nm lasers to excite mCherry driven by the *RCVRN* promoter (C, G, K). Composite images represent the merger of all three fluorescent signals (D, H, L). The eGFP signal was targeted to the cell membrane by a GAP43 tag to allow for visualization of ganglion cell axon bundles (white arrows in B, D). As organoids matured from D55 to D135, the number of cells expressing mCherry dramatically increased (compare C and K) and the $eGFP^+$ cells populated the interior of the organoid (J) while the $mCherry^+$ cells occupy the organoid periphery (K). Magnification Bar 100µm. Scanning parameters are in Table S9

Figure 4. Confirmation of PGP1-Derived Retinal Organoids Corresponded to the Appropriately Targeted Cell Types. At D55 (A-F, J-L) and D135 (G-I), the retinal organoids were dissociated into single cells, and used for FACS analysis. At D55, (A) the $Cerulean^+$ population was sorted from the $Cerulean^-$ population. RT-qPCR analysis revealed that the $Cerulean^+$ cells expressed significantly more Cerulean mRNA (B) and *VSX2* mRNA (C) than the $Cerulean^-$ cells. Also, at D55, (D) the $eGFP^+$ population was sorted from the $eGFP^-$ population. RT-qPCR analysis demonstrated that the $eGFP^+$ cells expressed significantly more eGFP mRNA (E) and *BRN3b* mRNA (F) than the $eGFP^-$ cells. At D135, (G) the $mCherry^+$ population was sorted from the $mCherry^-$ population. RT-qPCR analysis revealed that the $mCherry^+$ cells expressed significantly more mCherry mRNA (H) and *RCVRN* mRNA (I) than $mCherry^-$ cells. As a negative control, retinal organoids (D55) derived from WT hiPSC cells were run through the FACS and analyzed with the gates used for Cerulean (J), eGFP (K) and mCherry (L) with no cells occupying those gates. All RT-qPCR data was normalized to *GAPDH* expression. Error bars represent standard error of the mean (SE). Primer information listed in Table S7.

Figure 5. Retinal Development is Recapitulated in the Differentiating PGP1 hiPSC-Derived Retinal Organoids. (A-C) Undifferentiated PGP1 hiPSCs day 0 (D0, blue) and differentiated PGP1 retinal organoids at day 55 (D55, black) were used to measure mRNA levels of various markers via RT-qPCR normalized to *GAPDH*. (A) Expression of stem cell markers - *OCT4*, *NANOG*; (B) NRP markers - *PAX6, SIX3, LHX2*; (C) RPE markers - *MITF, BEST1*. (D-F) PGP1 hiPSCs at D0 and hiPSCs retinal organoids at D55, D95, and D166 of differentiation were used to measure mRNA levels via RT-qPCR normalized to *GAPDH*. (D) NRP and bipolar marker - *VSX2*; (E) RGC marker - *BRN3b*; and (F) PR marker – *RCVRN*. As organoid differentiation progressed from D0 to D55, stem cell markers significantly decreased and markers of retina and RPE differentiation significantly increased. Compared to D55, the PR marker *RCVRN* progressively increased in their mRNA expression, while the NRP marker – *VSX2* and the RGC marker – *BRN3b* gradually decreased in the older retinal organoids. Error bars represent standard error of the mean (SE), pair *t test* *$p<0.05$, **$p<0.005$, and ***$p<0.0005$). Primer information is listed in supplemental Table S5.

Figure 6. Retinal Organoids Differentiated from PGP1 Line Contain All Major Retinal Cell Types. At D55 of retinal organoid differentiation, the organoids were analyzed by immunohistochemistry using antibodies for the eye-field precursor marker RX (A), neuronal markers: PAX6 (B), SIX3 (C), the NRP marker VSX2 (D), the proliferation marker MCM2 (E), and the RGC marker BRN3 (F). At D70 of the retinal organoid differentiation, the organoids contain the amacrine cell marker AP2-α (G) and the photoreceptor marker RCVRN (H). The organoids contain the horizontal cell marker PROX-1 (I) at D95, and the Müller glia cell marker CRALBP (J) at D163. Also, at D163, the organoids contain the bipolar cell marker VSX2+/MCM2- (K, L). (L) is an enlarged view of the boxed area in (K) where VSX2+/MCM2+

(white arrowheads) cells represent NRPs and the VSX2+/MCM2- (white arrows) cells represent bipolar cells at D163. Dotted lines emphasize that the major expression domains of Brn3b (F), AP2α (G) and Prox1 (I) appear on the interior of the organoids while RCVRN (H) is predominantly on the organoid periphery. Magnification Bar 100 μm (A-K), 25μm (L). Antibodies used for immunohistochemistry listed in Supplemental Table S6.

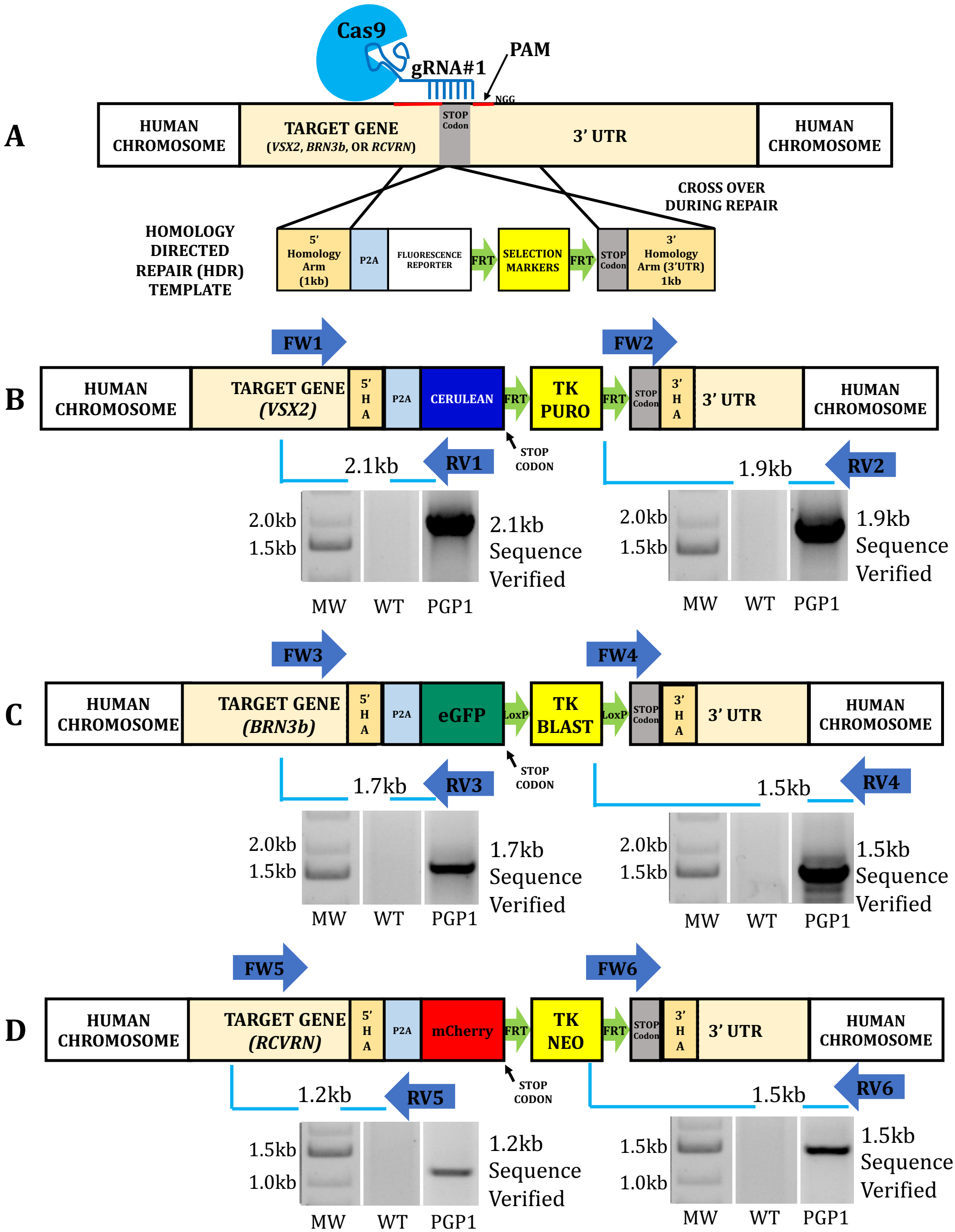
A
Cas9
gRNA#1
PAM
NGG
HUMAN CHROMOSOME
TARGET GENE (VSX2, BRN3b, OR RCVRN)
STOP Codon
3' UTR
HUMAN CHROMOSOME
CROSS OVER DURING REPAIR
HOMOLOGY DIRECTED REPAIR (HDR) TEMPLATE
5' Homology Arm (1kb)
P2A
FLUORESCENCE REPORTER
FRT
SELECTION MARKERS
FRT
STOP Codon
3' Homology Arm (3'UTR) 1kb
B
FW1
FW2
HUMAN CHROMOSOME
TARGET GENE (VSX2)
5' H A
P2A
CERULEAN
FRT
TK PURO
FRT
STOP Codon
3' H A
3' UTR
HUMAN CHROMOSOME
STOP CODON
2.1kb
RV1
2.0kb
1.5kb
2.1kb Sequence Verified
MW
WT
PGP1
1.9kb
RV2
2.0kb
1.5kb
1.9kb Sequence Verified
MW
WT
PGP1
C
FW3
FW4
HUMAN CHROMOSOME
TARGET GENE (BRN3b)
5' H A
P2A
eGFP
LoxP
TK BLAST
LoxP
STOP Codon
3' H A
3' UTR
HUMAN CHROMOSOME
STOP CODON
1.7kb
RV3
2.0kb
1.5kb
1.7kb Sequence Verified
MW
WT
PGP1
1.5kb
RV4
2.0kb
1.5kb
1.5kb Sequence Verified
MW
WT
PGP1
D
FW5
FW6
HUMAN CHROMOSOME
TARGET GENE (RCVRN)
5' H A
P2A
mCherry
FRT
TK NEO
FRT
STOP Codon
3' H A
3' UTR
HUMAN CHROMOSOME
STOP CODON
1.2kb
RV5
1.5kb
1.0kb
1.2kb Sequence Verified
MW
WT
PGP1
1.5kb
RV6
1.5kb
1.0kb
1.5kb Sequence Verified
MW
WT
PGP1

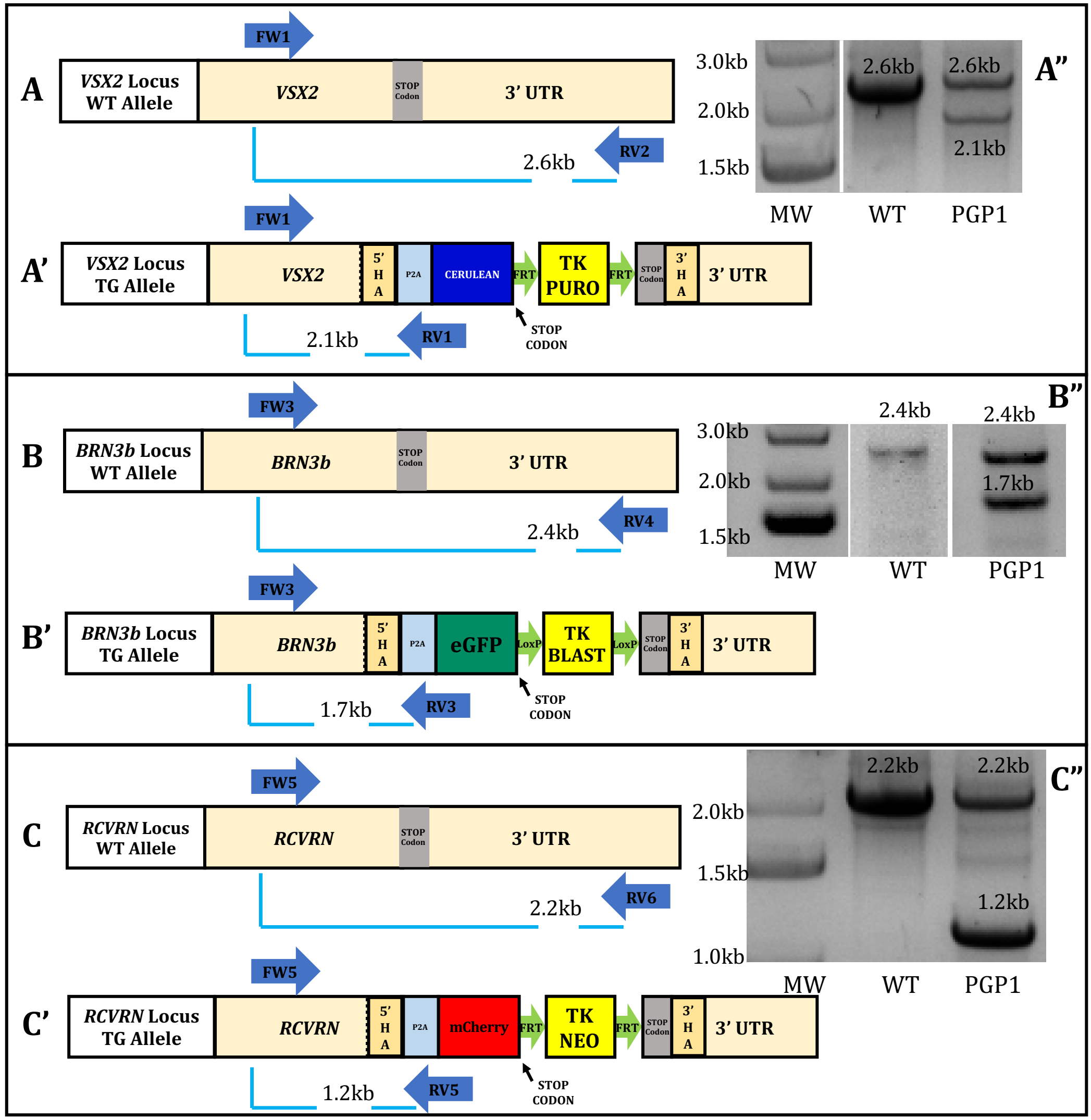
A
VSX2 Locus WT Allele
VSX2
STOP Codon
3' UTR
FW1
RV2
2.6kb
A'
VSX2 Locus TG Allele
VSX2
5' H A
P2A
CERULEAN
FRT
TK PURO
FRT
STOP Codon
3' H A
3' UTR
FW1
RV1
2.1kb
STOP CODON
A"
3.0kb
2.0kb
1.5kb
2.6kb
2.6kb
2.1kb
MW
WT
PGP1
B
BRN3b Locus WT Allele
BRN3b
STOP Codon
3' UTR
FW3
RV4
2.4kb
B'
BRN3b Locus TG Allele
BRN3b
5' H A
P2A
eGFP
LoxP
TK BLAST
LoxP
STOP Codon
3' H A
3' UTR
FW3
RV3
1.7kb
STOP CODON
B"
3.0kb
2.0kb
1.5kb
2.4kb
2.4kb
1.7kb
MW
WT
PGP1
C
RCVRN Locus WT Allele
RCVRN
STOP Codon
3' UTR
FW5
RV6
2.2kb
C'
RCVRN Locus TG Allele
RCVRN
5' H A
P2A
mCherry
FRT
TK NEO
FRT
STOP Codon
3' H A
3' UTR
FW5
RV5
1.2kb
STOP CODON
C"
2.0kb
1.5kb
1.0kb
2.2kb
2.2kb
1.2kb
MW
WT
PGP1

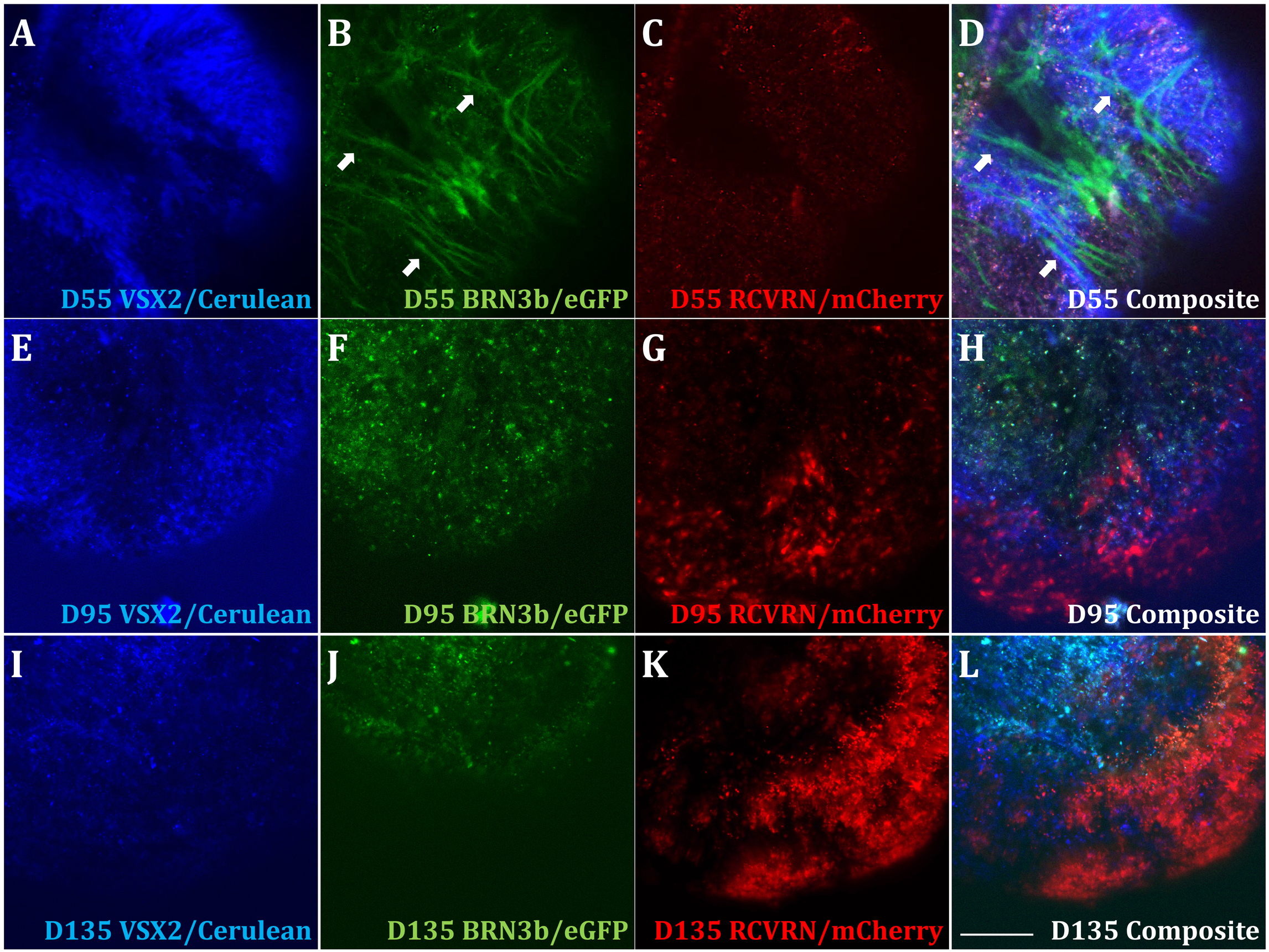
A
D55 VSX2/Cerulean
B
D55 BRN3b/eGFP
C
D55 RCVRN/mCherry
D
D55 Composite
E
D95 VSX2/Cerulean
F
D95 BRN3b/eGFP
G
D95 RCVRN/mCherry
H
D95 Composite
I
D135 VSX2/Cerulean
J
D135 BRN3b/eGFP
K
D135 RCVRN/mCherry
L
D135 Composite

FACS for Cerulean - PGP1 D55 Retina Cups

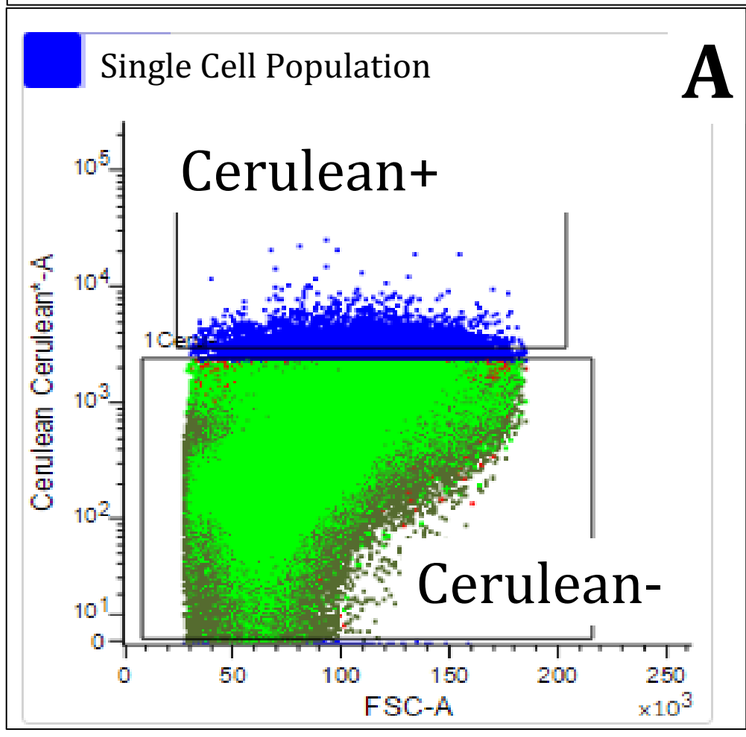

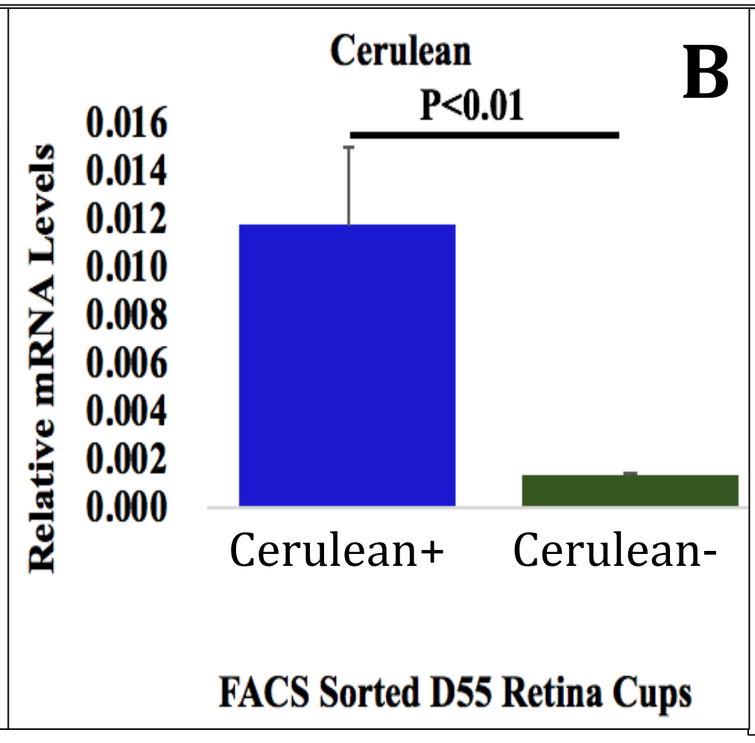

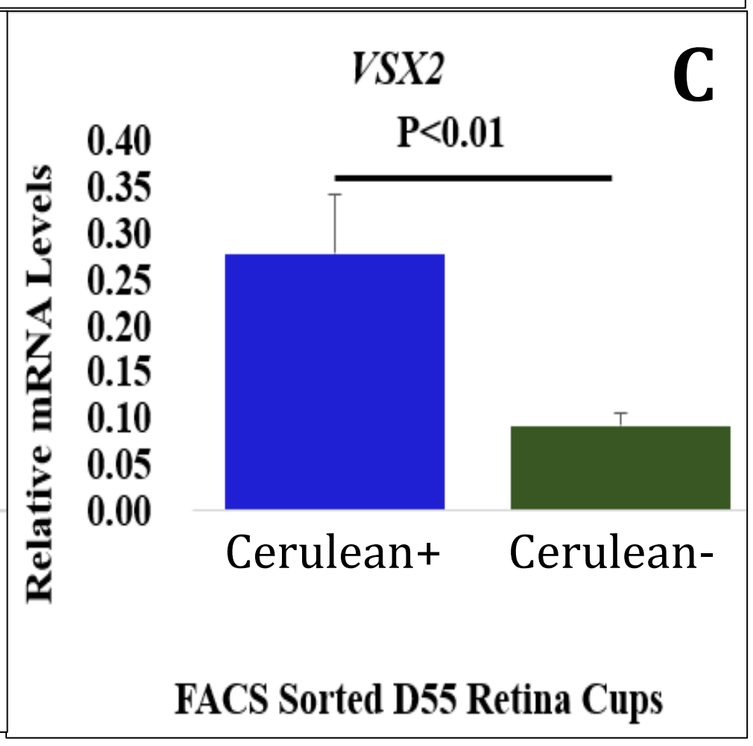

FACS for eGFP - PGP1 D55 Retina Cups

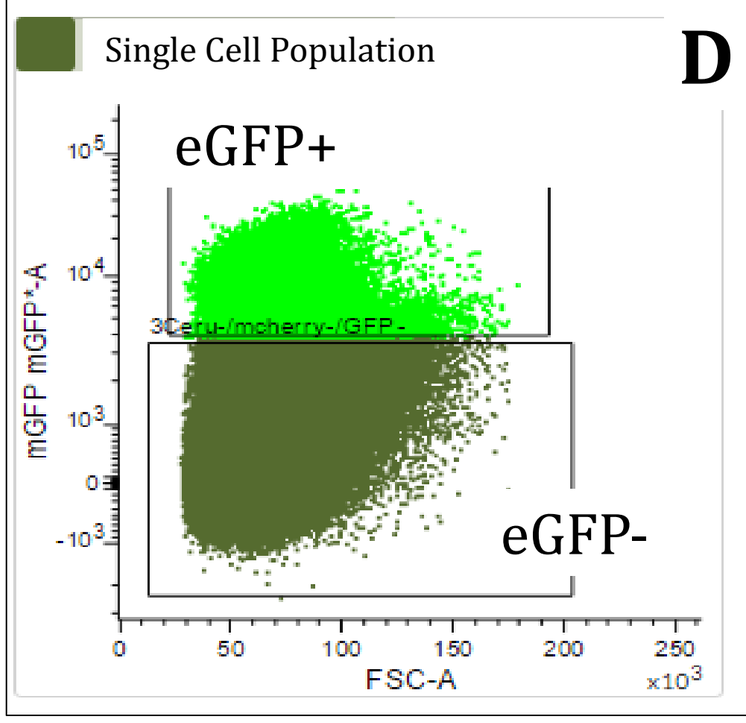

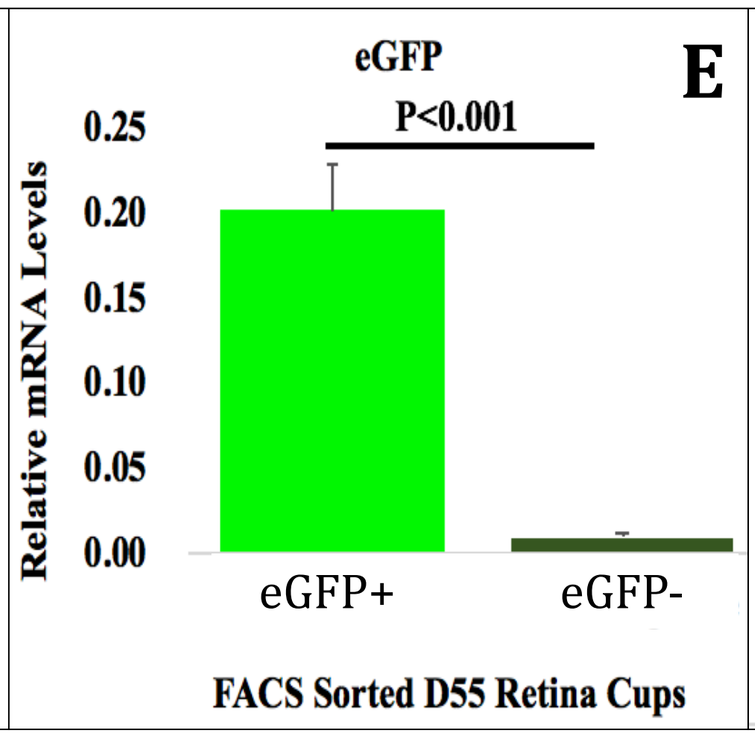

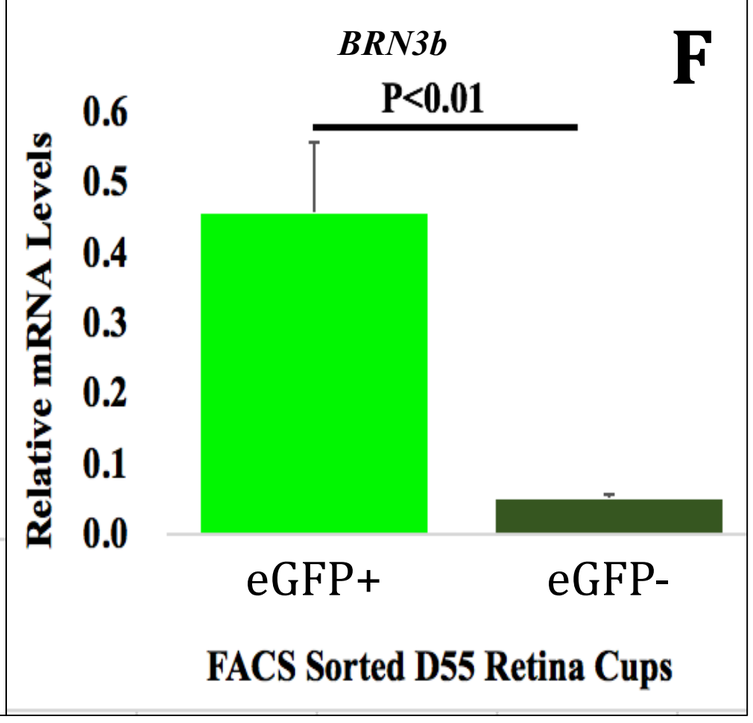

FACS for mCherry - PGP1 D135 Retina Cups

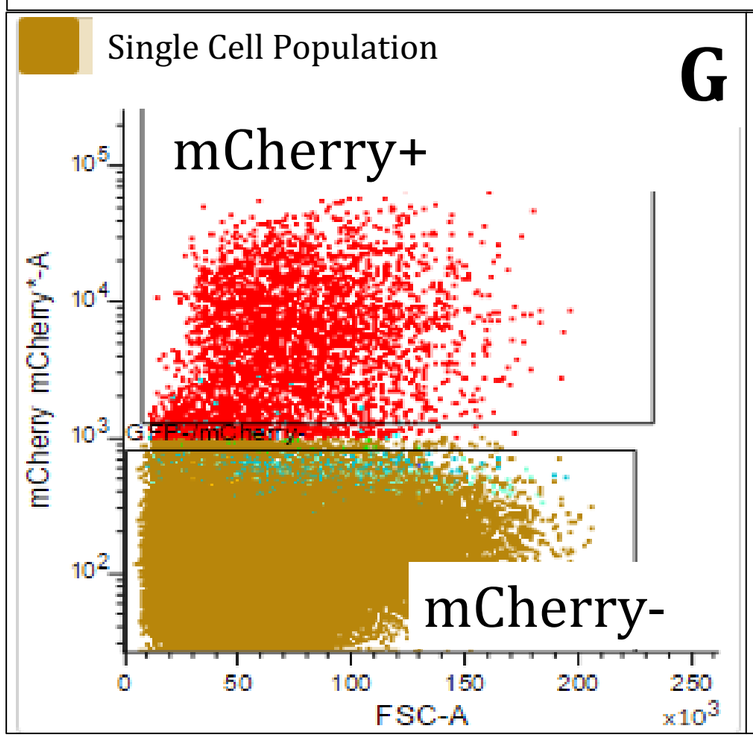

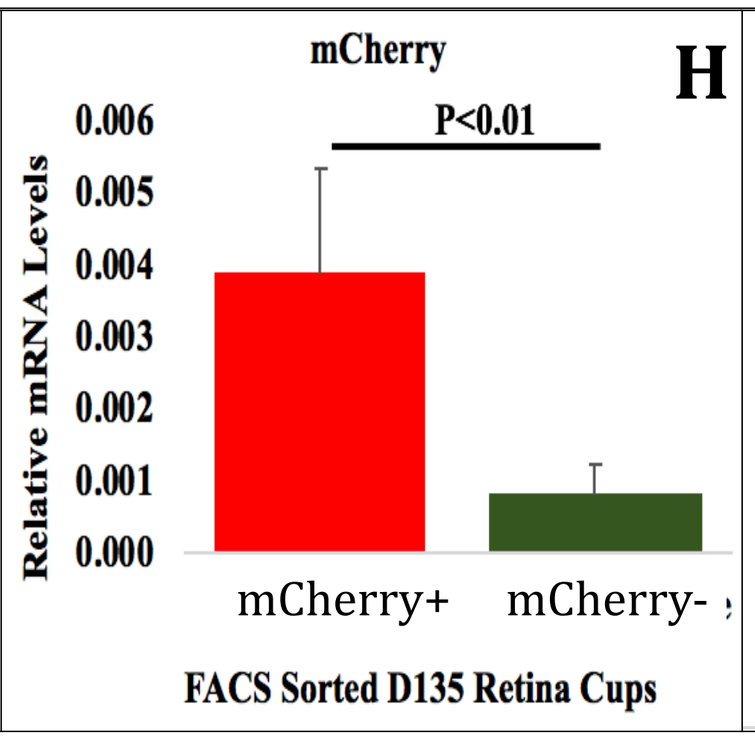

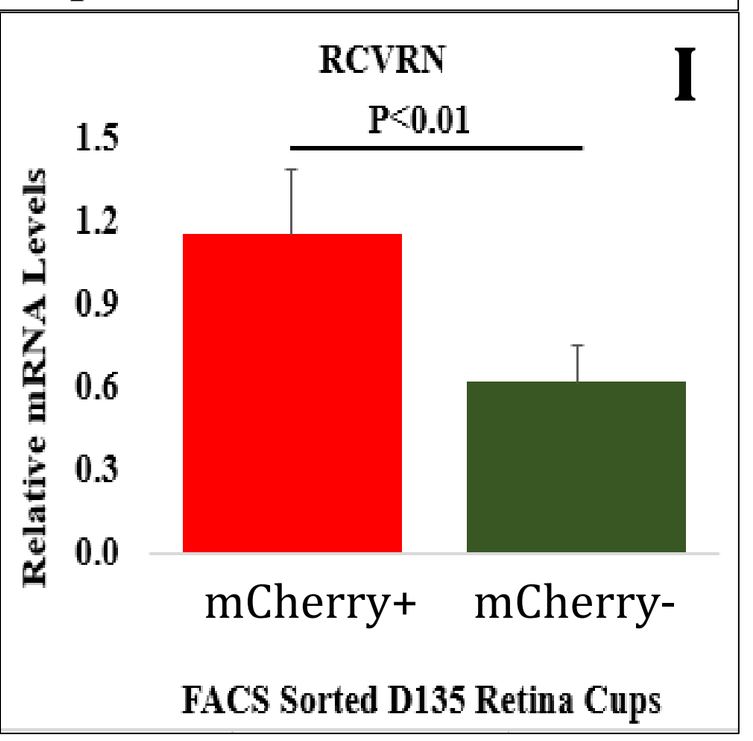

FACS Gating Control - D55 Retina Cups from Wild Type iPSC

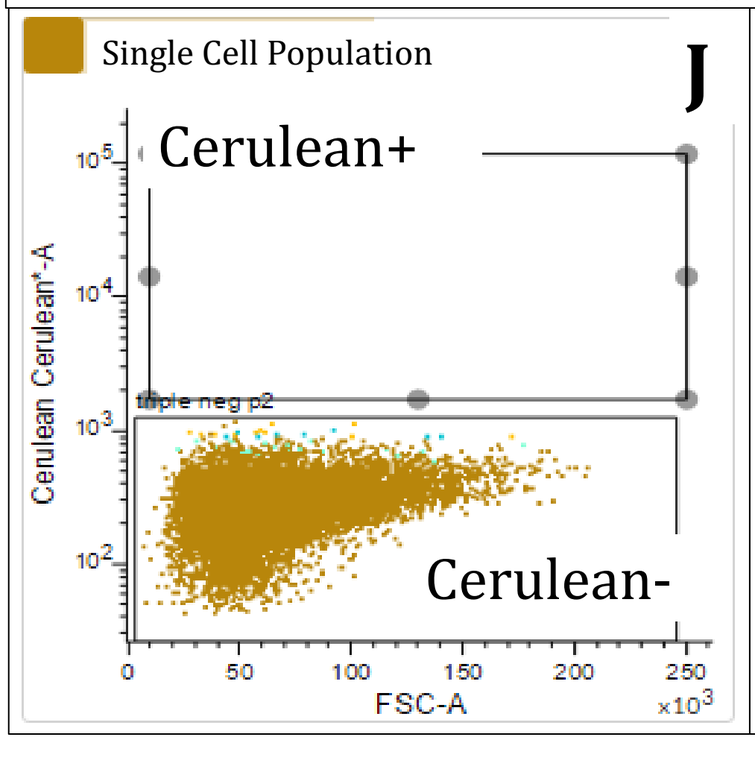

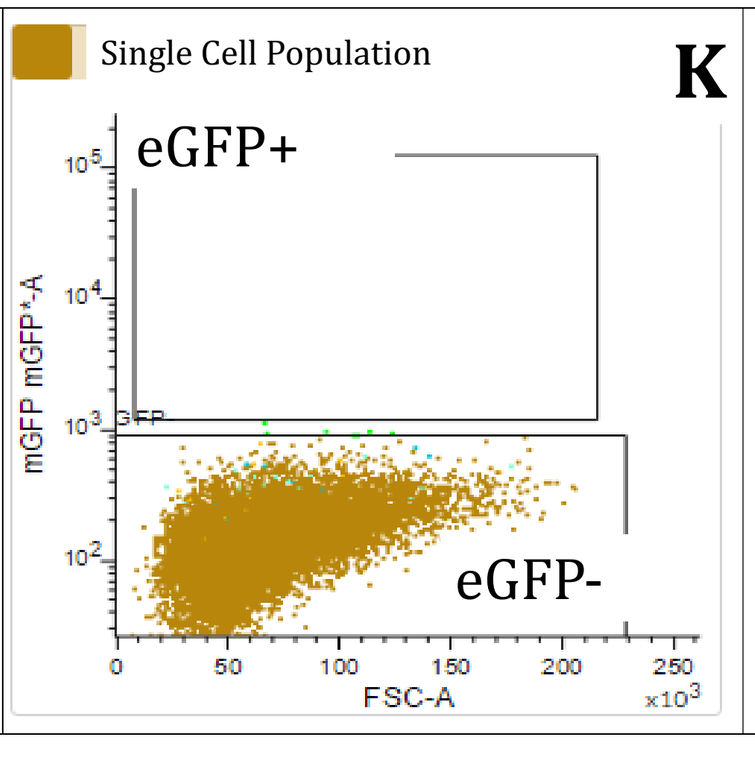

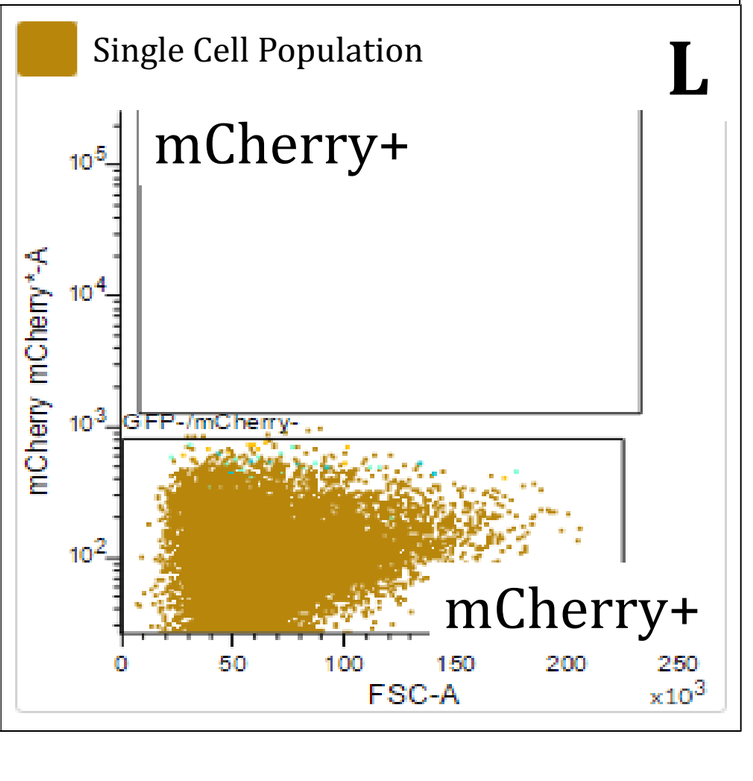

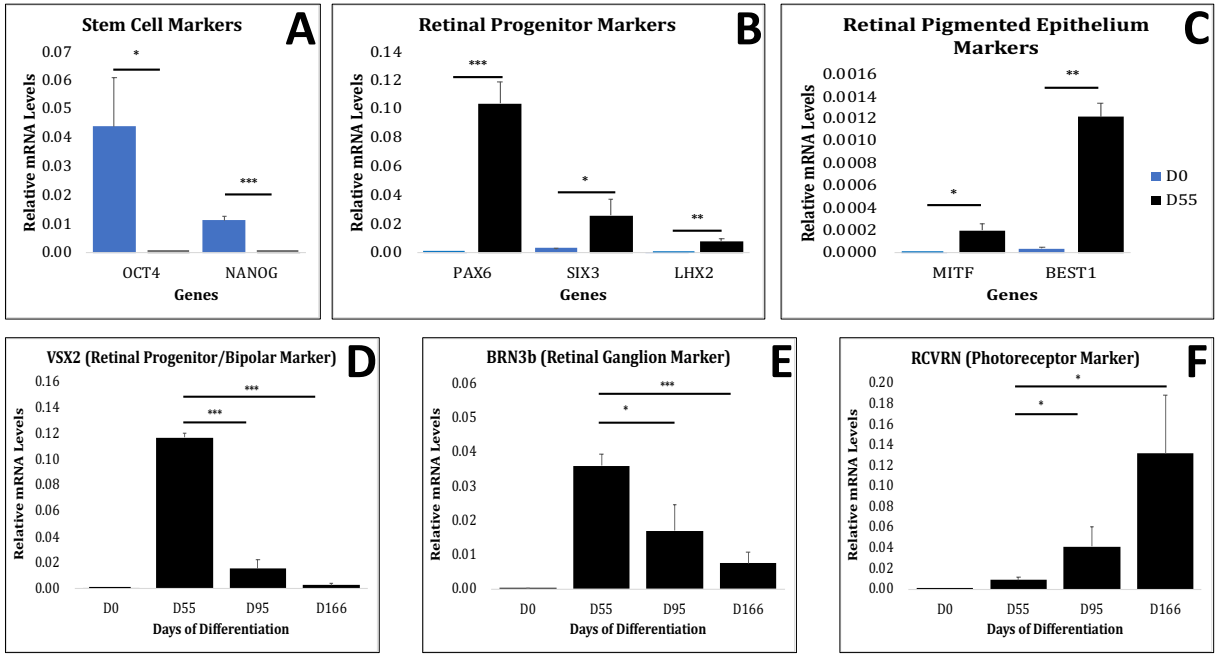
Stem Cell Markers
A
Relative mRNA Levels
0.07
0.06
0.05
0.04
0.03
0.02
0.01
0.00
*
***
OCT4
NANOG
Genes
Retinal Progenitor Markers
B
Relative mRNA Levels
0.14
0.12
0.10
0.08
0.06
0.04
0.02
0.00
***
*
**
PAX6
SIX3
LHX2
Genes
Retinal Pigmented Epithelium Markers
C
Relative mRNA Levels
0.0016
0.0014
0.0012
0.0010
0.0008
0.0006
0.0004
0.0002
0.0000
*
**
MITF
BEST1
Genes
D0
D55
VSX2 (Retinal Progenitor/Bipolar Marker)
D
Relative mRNA Levels
0.16
0.14
0.12
0.10
0.08
0.06
0.04
0.02
0.00
***
***
D0
D55
D95
D166
Days of Differentiation
BRN3b (Retinal Ganglion Marker)
E
Relative mRNA Levels
0.06
0.05
0.04
0.03
0.02
0.01
0.00
***
*
D0
D55
D95
D166
Days of Differentiation
RCVRN (Photoreceptor Marker)
F
Relative mRNA Levels
0.20
0.18
0.16
0.14
0.12
0.10
0.08
0.06
0.04
0.02
0.00
*
*
D0
D55
D95
D166
Days of Differentiation

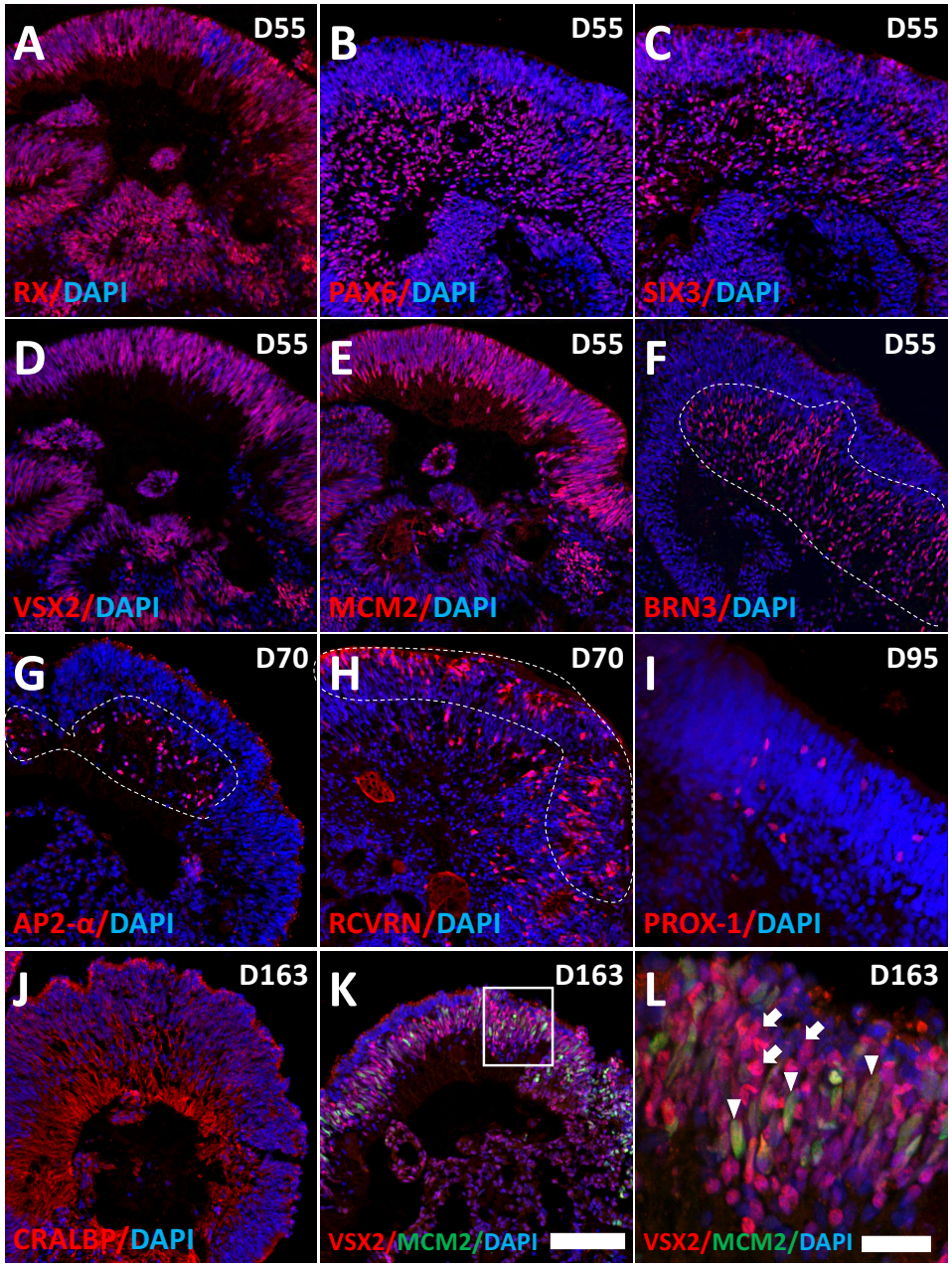
A
D55
RX/DAPI
B
D55
PAX6/DAPI
C
D55
SIX3/DAPI
D
D55
VSX2/DAPI
E
D55
MCM2/DAPI
F
D55
BRN3/DAPI
G
D70
AP2-α/DAPI
H
D70
RCVRN/DAPI
I
D95
PROX-1/DAPI
J
D163
CRALBP/DAPI
K
D163
VSX2/MCM2/DAPI
L
D163
VSX2/MCM2/DAPI